Electronic Supporting Information

Hierarchical assembly of ultrathin hexagonal SnS_2 nanosheets onto electrospun TiO_2 nanofibers: Enhanced photocatalytic activity based on photoinduced interfacial charge transfer

Zhenyi Zhang, Changlu Shao,* Xinghua Li, Yangyang Sun, Mingyi Zhang, Jingbo Mu, Peng Zhang, Zengcai Guo, and Yichun Liu

Center for Advanced Optoelectronic Functional Materials Research, and Key Laboratory of UV Light-Emitting Materials and Technology of Ministry of Education, Northeast Normal University, 5268 Renmin Street, Changchun 130024, People's Republic of China

*Corresponding author:
Center for Advanced Optoelectronic Functional Materials Research, and Key Laboratory of UV Light-Emitting Materials and Technology of Ministry of Education, Northeast Normal University, 5268 Renmin Street, Changchun 130024, People's Republic of China
E-mail: clshao@nenu.edu.cn; Tel. 8643185098803.

Measurement of photocatalytic activity:

The photocatalytic activies of the as-fabricated SnS_2/TiO_2 hierarchical nanostructures were evaluated by the degradation of target pollutants, including organic dyes (Rhodamine B (RhB) and Methyl orange (MO)) and phenols (4-nitrophenol (4-NP)), under UV and visible light irradiation, respectively. The 50 W high pressure mercury lamp (λ>313 nm) and 150 W high pressure xenon lamp with a cut-off glass filter transmitting (λ>420 nm) were used as UV and visible light sources, respectively. The photo-reactor was designed with an internal light source surrounded by a water-cooling quartz jacket to cool the lamp. In a typical process, a certain quality of photocatalysts (0.01 g for the UV light photocatalytic reaction and 0.05 g for the visible light photocatalytic reaction) were added into 100 mL of solution containing one of the above organic dyes or phenols with an initial concentration of 10 mg L^{-1}. The solution was stirred in the dark for 30 min to obtain a good dispersion and establish adsorption–desorption equilibrium between the above pollutants and the photocatalysts surface before the light irradiation. During the irradiation, 4 mL of the reaction solution were sampled at the given time intervals and centrifuged to remove the catalysts and were then analyzed by a Cary 500 UV-vis-NIR spectrophotometer. The degradability of the above pollutants was represented by C/C_0, where C_0 and C denoted the main absorption peak intensities of the above pollutants (RhB at 553 nm, MO at 463 nm, and 4-NP at 317 nm) before and after photocatalytic reaction. Photocatalytic activity of several reference samples, including TiO_2 (A) nanofibers, TiO_2 (AR) nanofibers, and SnS_2 nanosheets, were also measured by the same method.

Analysis of hydroxyl radicals:

Experimental procedures for analysis of hydroxyl radicals ($OH^{\bullet}$) were as follow:[1] 0.02 g

of the as-fabricated products was dispersed in a 100 mL of the 5×10^{-4} M terephthalic acid aqueous solution with a concentration of 2×10^{-3} M NaOH at ambient temperature. Fluorescence spectra of the generated 2-hydroxyterephthalic acid were measured on a LS-45/55 fluorescence spectrophotometer. After visible light irradiation for every 1 h, the reaction solution was filtrated to measure the increase in the Fluorescence intensity at 425 nm of 2-hydroxyterephthalic acid excited by 315 nm light.

Characterization:

X-ray diffraction (XRD) measurements were carried out using a D/max 2500 XRD spectrometer (Rigaku) with a Cu Kα line of 0.1541 nm. Scanning electron microscopy (SEM; XL-30 ESEM FEG, Micro FEI Philips) and high-resolution transmission electron microscopy (HRTEM; JEOL JEM-2100) were used to characterize the morphologies of the products. Energy dispersive X-ray (EDX) spectroscopy being attached to scanning electron microscopy (SEM) was used to analyze the composition of products. X-ray photoelectron spectroscopy (XPS) was performed on a VG-ESCALAB LKII instrument with a Mg Kα ADES ($h\nu$=1253.6 eV) source at a residual gas pressure below 10^{-8} Pa. UV-vis diffuse reflectance (DR) spectroscopy of the products were recorded on a Cary 500 UV-vis-NIR spectrophotometer. The photoluminescence (PL) spectra of the as-fabricated products were detected with a Jobin Yvon HR800 micro-Raman spectrometer using a 325 or 488 nm line from a He-Cd laser. Fourier transform infrared spectroscopy (FT-IR) spectra were obtained on Magna 560 FT-IR spectrometer with a resolution of 1 cm^{-1}. Surface photovoltage spectroscopy (SPS) instrument was carried out on a self-made instrument. Monochromatic light was obtained by passing light from a 500 W xenon lamp (CHF XQ500W, Global xenon lamp power) through a double-prism monochromator (Hilger and Watts, D 300). The slit

width of entrance and exit is 1 mm. A lock-in amplifier (SR830-DSP), synchronized with a light chopper (SR540) was employed to amplify the photovoltage signal. The range of modulating frequency is from 20 to 70 Hz. The spectral resolution is 1 nm. The raw SPS data were normalized using the illuminometer (Zolix UOM-1S). During the measurement process, the sample was put between two indium tin oxide (ITO) electrodes to form a sandwich structured photovoltage cell. It was ensured that the light penetrating depth was much less than the sample layer thickness.

Phase Content:

The phase content of anatase and rutile in the as-electrospun TiO_2 nanofibers before and after hydrothermal treatment were calculated from the respective peak intensities of anatase (101) and rutile (110) with the equation:[2]

$$W_R = \frac{I_R}{0.884 I_A + I_R}$$

Where W_R was the weight fraction of rutile; I_A and I_R were the integrated intensities of anatase (101) and rutile (110) peak, respectively.

Grain size:

The average grain sizes of the as-electrospun TiO_2 nanofibers before and after hydrothermal treatment were calculated by applying the Debye–Scherrer formula on the anatase (101) and rutile (110) diffraction peaks, respectively:[3]

$$d = \frac{K\lambda}{B\cos\theta}$$

Where d was the average grain size; K was a constant (0.89); λ was the wavelength of the X-ray radiation (Cu Kα = 0.1541 nm); B was the full-width at half maximum (FWHM); θ was the diffraction angle.

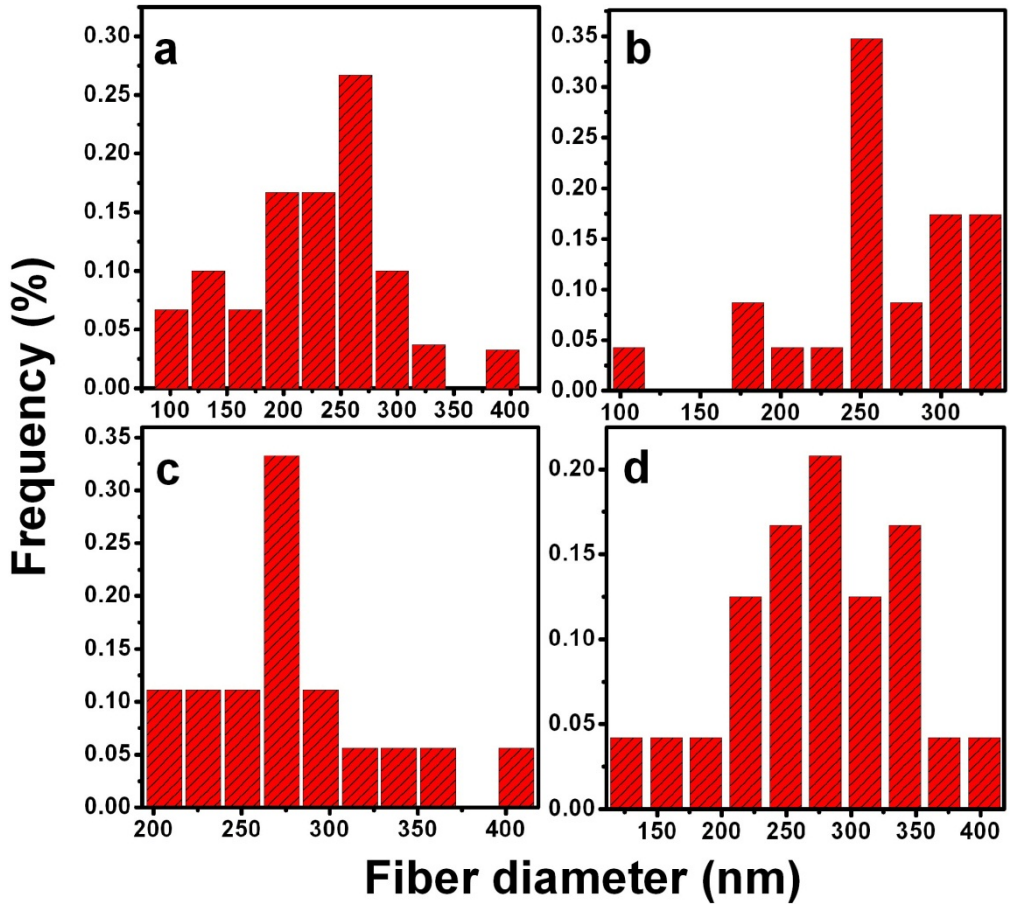

Figure S1. Diameter distribution histograms of the as-fabricated products: (a) TiO_2 (A) nanofibers; (b) SnS_2/TiO_2 (A) hierarchical nanostructures; (c) TiO_2 (AR) nanofibers; (d) SnS_2/TiO_2 (AR) hierarchical nanostructures.

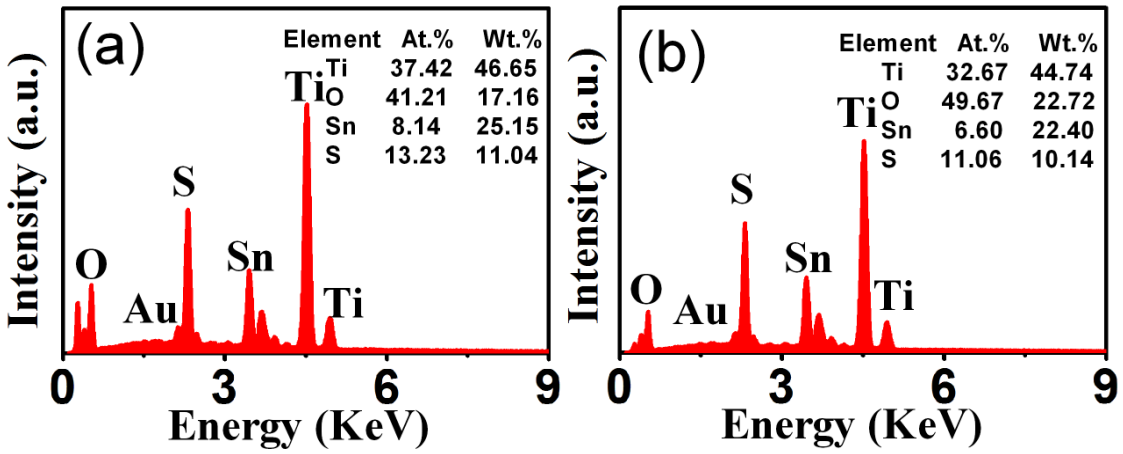

Figure S2. EDX spectrum of (a) SnS_2/TiO_2 (A) hierarchical nanostructures and (b) SnS_2/TiO_2 (AR) hierarchical nanostructures detected in Figure 2b and d, respectively.

Table S1. Physicochemical properties of the as-fabricated products

Sample	Grain size (nm)		Phase content (wt.%)		Diameter (nm)
	Anatase	Rutile	Anatase	Rutile	
TiO_2 (A) nanofibers	17.08	-----	100	0	112-346
TiO_2 (AR) nanofibers	17.25	17.03	19.8	81.2	111-395
SnS_2/TiO_2 (A) hierarchical nanostructures	17.14	-----	100	0	115-371
SnS_2/TiO_2 (AR) hierarchical nanostructures	17.36	17.25	19.5	81.5	164-366

Table S2. Core-level binding energy of the elements in the as-fabricated products.

Sample	Binding Energy (eV)											
	Ti $2p_{3/2}$	Ti $2p_{1/2}$	O 1s				Sn $3d_{5/2}$		Sn $3d_{3/2}$		S $2p_{3/2}$	S $2p_{1/2}$
TiO_2 (A) nanofibers	458.55	464.28	529.87	——	531.62	532.90	————				————	
TiO_2 (AR) nanofibers	458.51	464.22	529.82	——	531.65	532.91	————				————	
SnS_2/TiO_2 (A) hierarchical nanostructures	458.65	464.40	529.89	531.37	531.63	532.95	485.76	486.34	494.19	494.75	160.90	162.12
SnS_2/TiO_2 (AR) hierarchical nanostructures	458.70	464.39	529.91	531.32	531.64	532.92	485.59	486.16	494.00	494.62	160.60	161.72
SnS_2 nanosheets	————		————				——	486.47	——	494.88	161.27	162.44

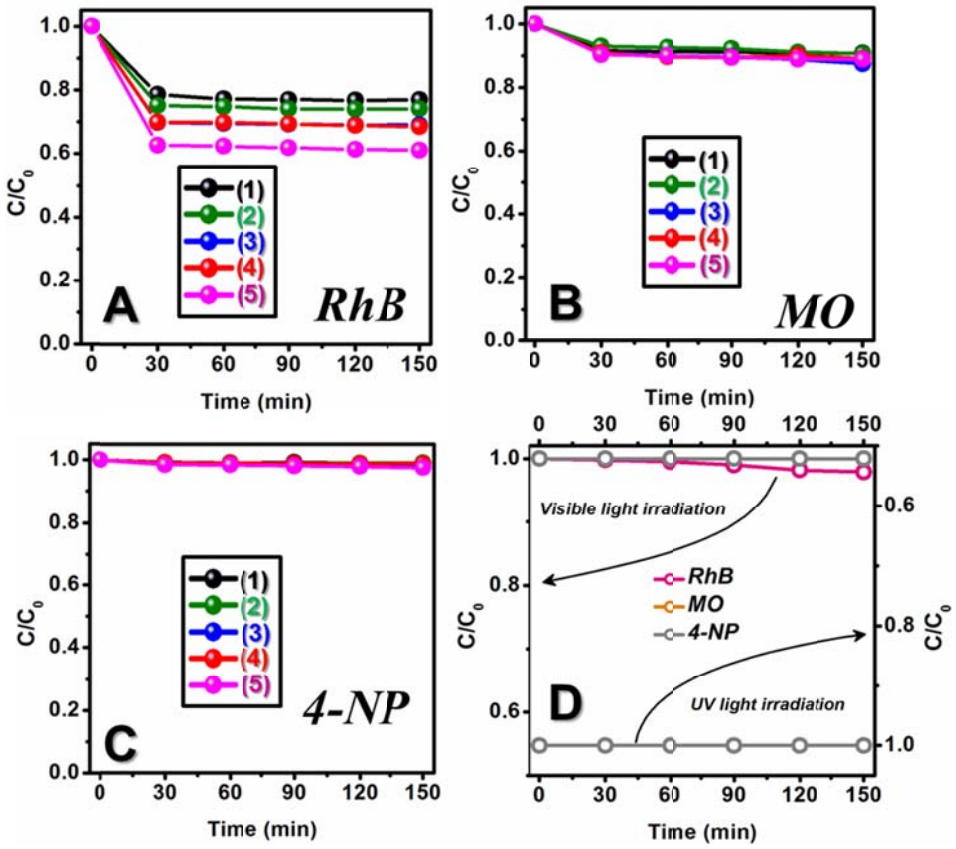

Figure S3. Degradation profiles of the target pollutants in the presence of the as-fabricated photocatalysts but in the dark: (A) RhB; (B) MO; (C) 4-NP; and (D) with UV or visible light irradiation but in the absence of the above photocatalysts: (1) TiO_2 (A) nanofibers; (2) TiO_2 (AR) nanofibers; (3) SnS_2/TiO_2 (A) hierarchical nanostructures; (4) SnS_2/TiO_2 (AR) hierarchical nanostructures; (5) SnS_2 nanosheets.

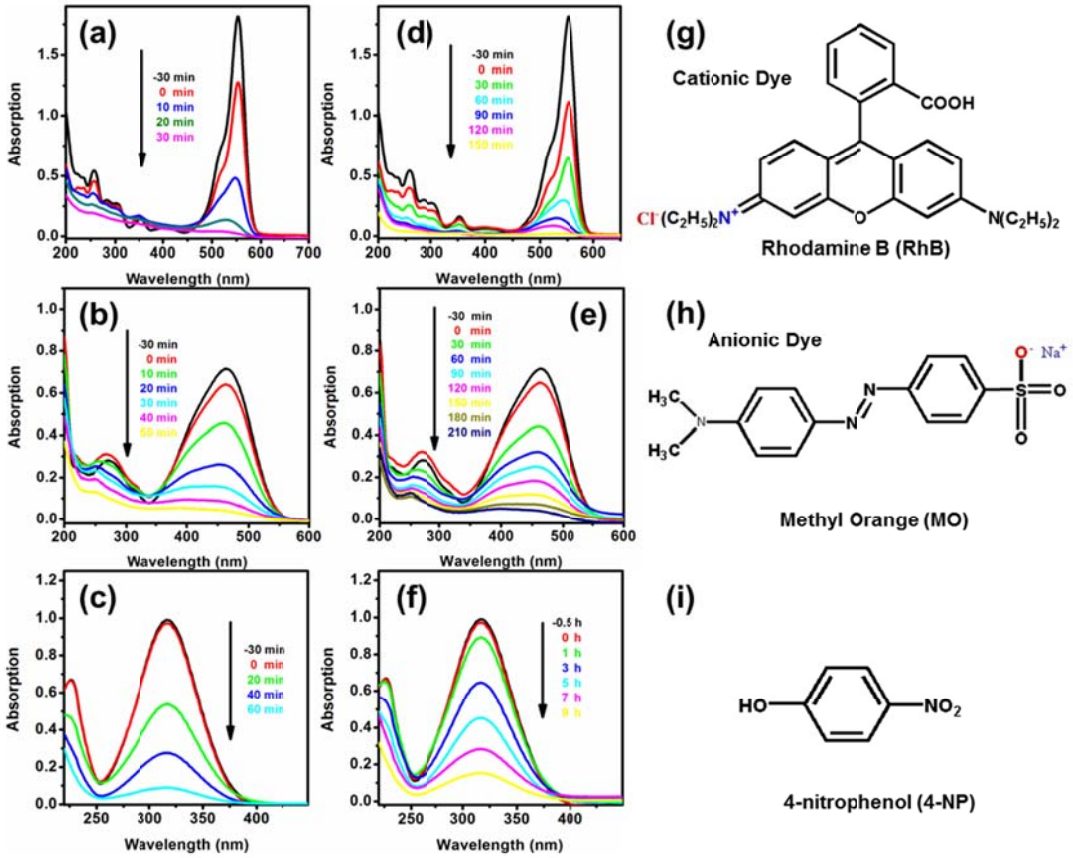

Figure S4. Adsorption spectra of the target pollutants solutions ((a, d) RhB; (b, e) MO; (c, f) 4-NP)) in the presence of SnS_2/TiO_2 (AR) hierarchical nanostructures under (a-c) UV or (d-f) visible light irradiation at different periods of time; Structural formula of (g) RhB, (h) MO, and (i) 4-NP.

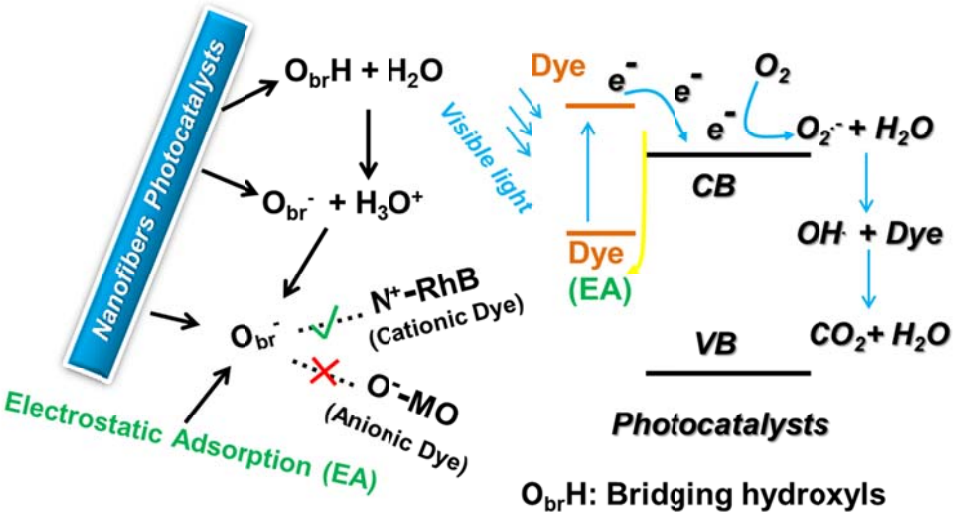

Figure S5. Schematic diagram of dye self-sensitized process in the presence of TiO_2 nanofibers photocatalysts under visible light irradiation.

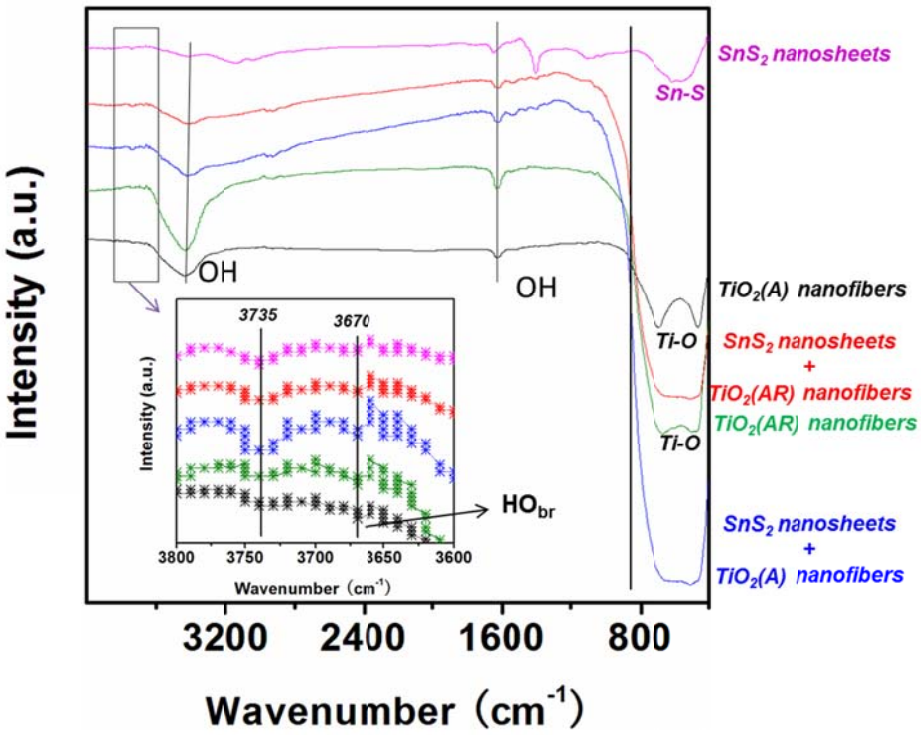

Figure S6. FT-IR spectra of the as-fabricated products: TiO_2 (A) nanofibers; TiO_2 (AR) nanofibers; SnS_2/TiO_2 (A) hierarchical nanostructures; SnS_2/TiO_2 (AR) hierarchical nanostructures; SnS_2 nanosheets.

Dye self-sensitized process:

The mechanism of the dyes photodegradation was proposed as follow:[4] under visible light excitation, the adsorbed dyes could be excited to generate the electrons, which then transfer to the conduction band (CB) of TiO_2. After that, dissolved oxygen molecules (O_2) reacted with the CB electrons (e^-) to yield superoxide radical anions ($O_2^{\bullet -}$), which on protonation generated the hydroperoxy radicals ($HO_2^{\bullet}$), producing hydroxyl radicals ($OH^{\bullet}$), which was a strong oxidizing agent to decompose the organic dyes.

Recently, Pan et al. reported very useful information about the dye sensitization of TiO_2. In that report, the water bonded to the surface bridging hydroxyls (HO_{br}) played an important role during the dye sensitization of TiO_2.[5] From the results of FT-IR spectra in Figure S6, it could be proven that the HO_{br} and basic terminal hydroxyl groups (HO_t) centered at 3670 and 3735 cm^{-1} were also existed on the surface of as-electrospun TiO_2 nanofibers. As illustrated in Figure S5, during the photocatalysis of TiO_2 nanofibers in the organic dyes aqueous solution, water could be bonded to HO_{br} via strong hydrogen bonding interactions ($H_2O\ldots HO_{br}$). Then, the solvation effect of adsorbed and the surrounding bulk water could enhance the polarization and acidity of HO_{br}, resulting in the formation of hydronium structures ($H_3O^+\ldots O_{br}^-$). It had been pointed out that the formation process of hydronium structures was very slow in air but obviously accelerated in bulk water. When the dye cations attached on the surface of TiO_2 nanofibers, they displaced H_3O^+ and formed the electrostatic adsorption mode ($O_{br}^-\ldots N^+$-dye). The electrostatic adsorption could induce ultrafast electrons transfer (ET) from the aromatic adsorbate to the CB of TiO_2 nanofibers, leading to the enhancing the sensitization under visible light irradiation. However, this effect should not be valid for anionic dyes, such as MO in our work. As observed in Figure S6, the adsorption peaks of

HO_{br} were also found in the FT-IR spectra of the SnS_2 nanosheets and SnS_2/TiO_2 hierarchical nanostructures. Thus, we believed that the dyes self-sensitized process also occurred on the visible light photocatalysis of the SnS_2 nanosheets and SnS_2/TiO_2 hierarchical nanostructures.

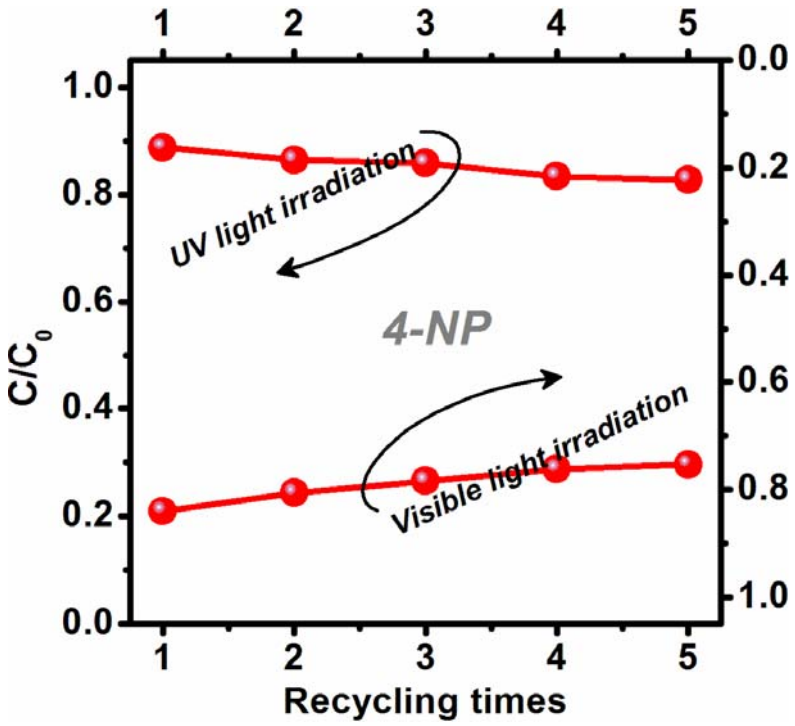

Figure S7. Photocatalytic activity of the SnS_2/TiO_2 (AR) hierarchical nanostructures for the degradation of 4-NP with five times of cycling uses.

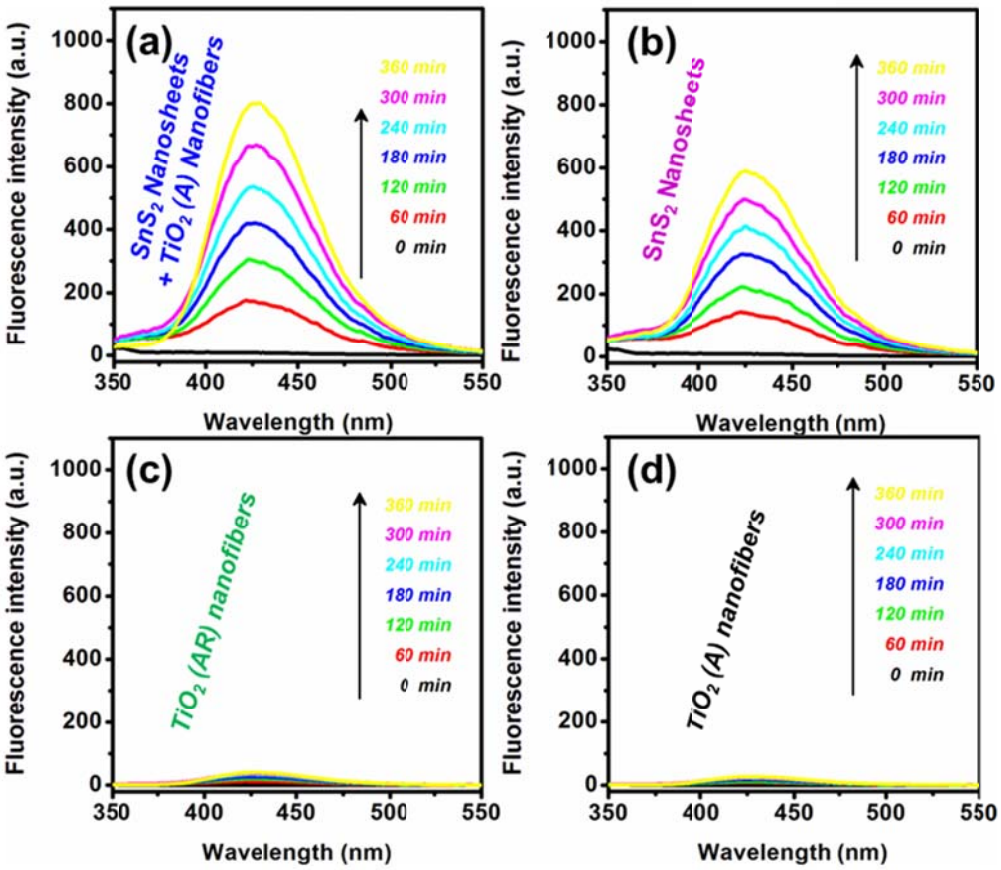

Figure S8. Fluorescence spectral changes observed during illumination of the as-fabricated products in terephthalic acid solution (under 315 nm excitation).

Table S3. Band gap energy positions of the as-fabricated products.

Semiconductors	Electronegativity (X)	Estimated E_g (eV)	Calculated CB position (eV)	Calculated VB position (eV)
SnS_2	5.47	2.48	-4.23	-6.71
Anatase TiO_2	5.81	3.10	-4.26	-7.36
Rutile TiO_2	5.81	<3.10	<-4.26	>-7.36

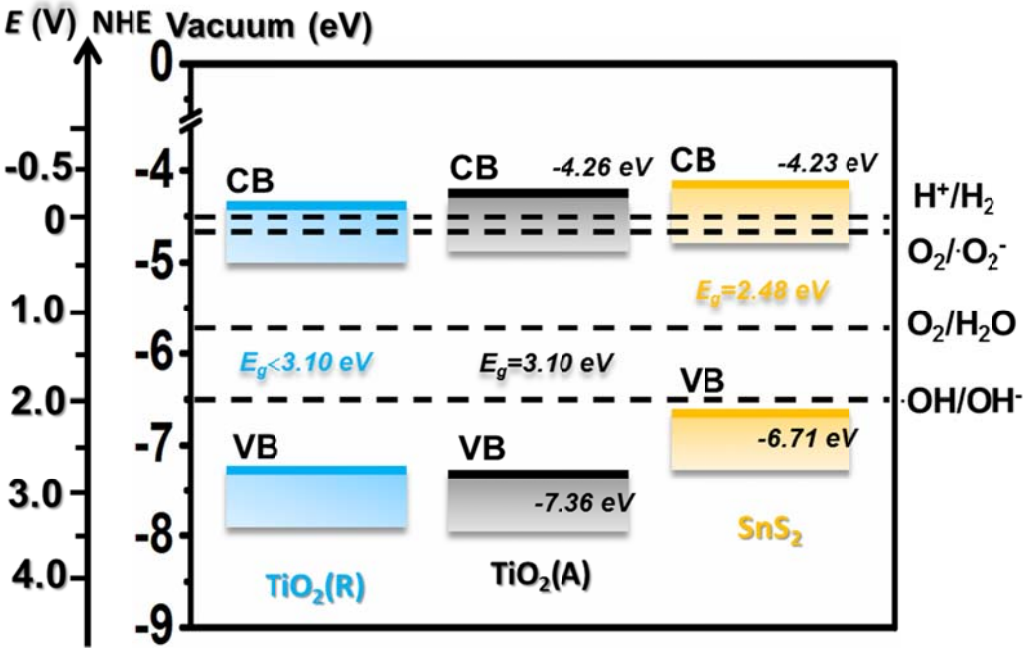

Scheme S1. The energy band diagram of SnS_2 nanosheets, TiO_2 (A) and TiO_2 (R) nanoparticles in the nanofibers at PH=7 in nonthermal equilibrium.

Calculation of conduction and valence band (CB and VB) edge positions:

The band edge positions of the CB and VB of the SnS_2 nanosheets, and anatase and rutile phase TiO_2 nanoparticles in the electrospun nanoifbers could be determined by the following empirical formula:[6]

$$E_{VB} = X - E^e + 0.5E_g \quad (1)$$

$$E_{CB} = X - E^e - 0.5E_g \quad (2)$$

where E_{VB} and E_{CB} were the valence and conduction band edges potential of the semiconductor, respectively; χ was the electronegativity of the semiconductor, expressed as the geometric mean of the absolute electronegativity of the constituent atoms, which was defined as the arithmetic mean of the atomic electron affinity and the first ionization energy. E^e was the energy of free electrons on the hydrogen scale (ca. 4.5 eV). E_g was the band gap of the semiconductor. Based on the above equations, the CB and VB edge positions of SnS_2 nanosheets in our experiment were calculated to be -0.27 and 2.21 V (-4.23 and -6.71 eV), respectively. Accordingly, the CB and VB edge positions of anatase TiO_2 nanoparticles in the electrospun nanofibers were about -0.24 and 2.86 V (-4.26 and -7.36 eV), respectively. In the case of rutile TiO_2 nanoparticles in the electrospun nanofibers, the CB and VB edge positions were >-0.24 V and <2.86 V (<-4.26 eV and >-7.36 eV), respectively. The calculated band positions of the above semiconductors were summarized in Table S3.

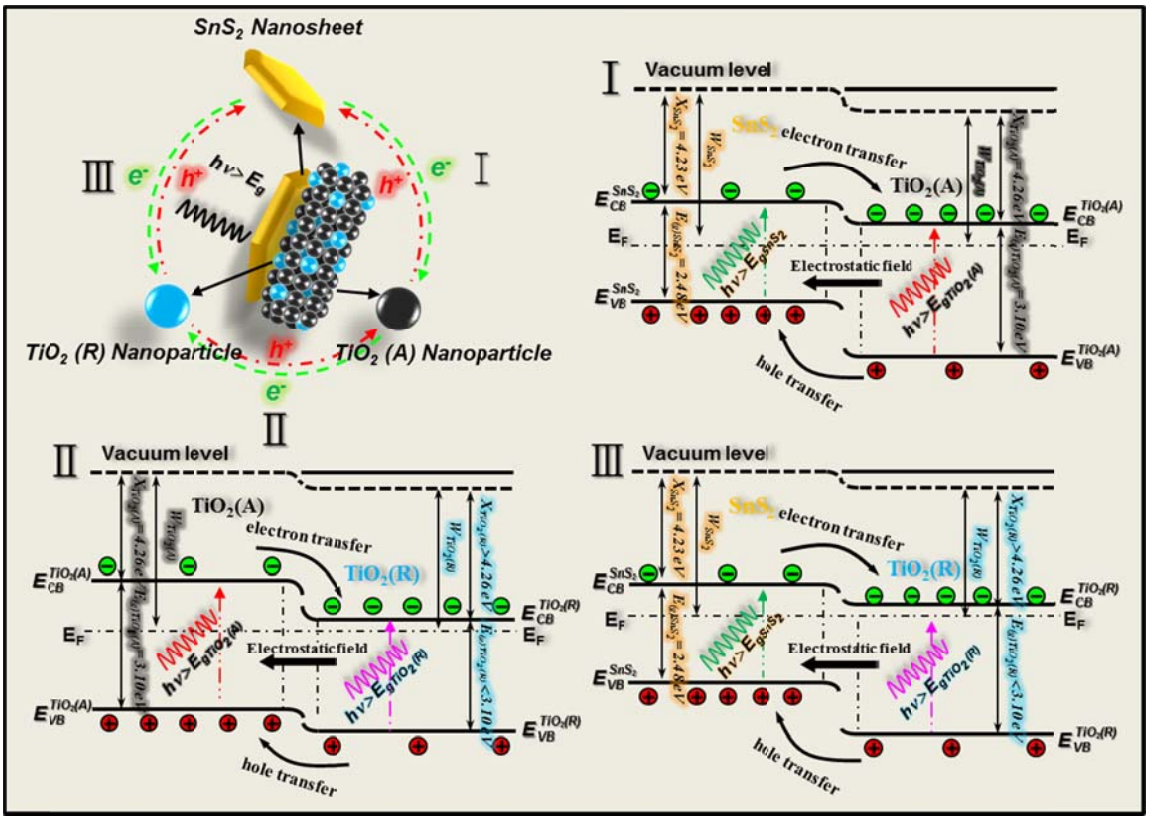

Scheme S2. Schematic diagram showing the energy band structure and photoinduced electron-hole pairs separation at the interface of (I) SnS_2/TiO_2 (A), (II) TiO_2 (A)/TiO_2 (R), and (III) SnS_2/TiO_2 (R) heterojunctions.

Photoinduced interfacial charge transfer:

There were about three kinds of interface in the tricomponent heterojunction system of SnS_2/TiO_2 (AR) hierarchical nanostructures: (I) SnS_2/TiO_2 (A), (II) TiO_2 (A)/TiO_2 (R), and (III) SnS_2/TiO_2 (R) heterojunction. On the basis of the above experimental results and the theory analysis, the proposed energy band structure diagrams of the above three kinds of heterojunction were elucidated schematically in Scheme S2. To understand the energy band structure of the above tricomponent heterojunction system, three relevant material properties of the SnS_2, anatase and rutile phase TiO_2, including the electron affinity, the band gap, and

the work function, should be given. In our experiment, the electron affinities of SnS_2 and anatase phase TiO_2 were about 4.23 and 4.26 eV, respectively. In the case of rutile phase TiO_2, the electron affinity was a little larger than 4.26 eV, but could not be given a certain value. The band gaps of the SnS_2 and anatase phase TiO_2 were about 2.48 and 3.10 eV, respectively. Similarly, the band gap for rutile phase TiO_2 in our experiment was below 3.10 eV. Furthermore, form the results of the XPS in Figure 5, it could be concluded that the work function of the SnS_2 was larger than that of the anatase or rutile phase TiO_2. Thus, the Fermi energy level of SnS_2 was lower than that of the anatase or rutile phase TiO_2. As observed in Scheme S2 I, when the SnS_2 nanosheets and anatase phase TiO_2 nanoparticles formed a heterojunction, the electron transfer could occur from the anatase phase TiO_2 nanoparticles to the SnS_2 nanosheets until the system attained equilibration. In addition, the Fermi energy level of the semiconductor was directly related to the number of accumulated electrons, as illustrated by the following:[7] $E_F = E_{CB} + kT \ln n_c / N_c$, where E_{CB} was the conduction band energy, n_c was the density of accumulated electrons, and N_c was the charge carrier density of the semiconductor. In the case of SnS_2 nanosheets/anatase phase TiO_2 nanoparticles heterojunction, a positive shift in the Fermi energy level of the SnS_2 and a negative shift in the Fermi energy level of the anatase phase TiO_2 would be expected. As a result, a new Fermi energy level was formed in the above heterojunction. Meanwhile, an electrostatic field was built in the discontinuity interface of SnS_2 and anatase phase TiO_2 because of the electron transfer, which could lead to the energy band and vacuum energy level bending. When the SnS_2/anatase phase TiO_2 heterojunction was excited by the light with a photon energy higher or equal to the band gaps of SnS_2 and anatase phase TiO_2, the electrons in the VB could be excited to the CB with simultaneous generation of the same amount of holes in the VB. From

the energy band structure diagram of the SnS_2/anatase phase TiO_2 heterojunction, it could be found that the photogenerated electron transfer occurred from the CB of SnS_2 to the CB of anatase phase TiO_2 and, conversely, the photogenerated hole transfer could take place from the VB of anatase phase TiO_2 to the VB of SnS_2, suggesting that the photogenerated electrons and holes were efficiently separated. Similarly, in Scheme S2 III, when the SnS_2 nanosheets and rutile phase TiO_2 nanoparticles formed a heterojunction, the electron transfer could occur from the rutile phase TiO_2 nanoparticles to the SnS_2 nanosheets until the system attained equilibration. Meanwhile, an electrostatic field was built in the discontinuity interface of SnS_2 and rutile phase TiO_2 due to the electron transfer. When the SnS_2/rutile phase TiO_2 heterojunction was radiated by the light with a photon energy higher or equal to the band gaps of SnS_2 and rutile phase TiO_2. The photogenerated electrons and holes were separated under the influence of the electrostatic field induced by different work functions. Accordingly, the photoinduced electrons moved to the rutile phase TiO_2 side and the photoinduced holes to the SnS_2 side. At last, in the case of the heterojunction interface between the anatase and rutile TiO_2 nanoparticles, the photoinduced electrons flew from anatase TiO_2 to rutile TiO_2 driven by the electrostatic field, while the photogenerated holes flew in the opposite direction from rutile TiO_2 to anatase TiO_2, as illustrated in Scheme S2II. Similarly, the charge separation driven by anatase/rutile TiO_2 heterojunction had been reported before in either double-layered film or composite powders.[8] On the whole, under UV light irradiation, the recombination efficiency of photoinduced electron–hole pairs should be reduced in the SnS_2/TiO_2 (AR) hierarchical nanostructures: the holes might be easily accumulated in the VB of SnS_2 nanosheets while the electrons might be easily accumulated in the CB of TiO_2 (R) nanoparticles in the TiO_2 nanofibers. However, under visible light irradiation, it was possible

to excite only the SnS_2 nanosheets supported on the TiO_2 electrospun nanofibers, and generated the photoinduced electrons and holes on its CB and VB, respectively. Induced by the electrostatic field existed in the interface of SnS_2/TiO_2 (A), TiO_2 (A)/TiO_2 (R), and SnS_2/TiO_2 (R) heterojunction, the photoinduced electrons could readily transfer from the CB of SnS_2 nanosheets to the CB of TiO_2 (A) nanoparticles, and then (or) diffused to the CB of TiO_2 (R) nanoparticles via interface, whereas the photoinduced holes still remained on the VB of SnS_2 nanosheets. Therefore, the photoinduced charge carriers in SnS_2 nanosheets could be effectively separated, and accordingly their recombination was slowed down.

Reference:

1. K. Ishibashi, A. Fujishima, T. Watanabe and K. Hashimoto, *Electrochem. Commun.*, 2000, **2**, 207-210.
2. H. Zhang and J. F. Banfield, *J. Phys. Chem. B*, 2000, **104**, 3481-3487.
3. Z, Zhang, C. Shao, X. Li, C. Wang, M. Zhang and Y. Liu, *ACS Appl. Mater. Interfaces*, 2010, **2**, 2915-2923.
4. (a) Z. Xiong, L. L. Zhang, J. Ma and X. S. Zhao, Chem. Commun., 2010, 46, 6099-6101; (b) C. Chen, W. Ma and J. Zhao, Chem. Soc. Rev., 2010, 39, 4206-4219; (c) D. Zhao, C. Chen, Y. Wang, W. Ma, J. Zhao, T. Rajh and L. Zang, *Environ. Sci. Technol.*, 2008, **42**, 208-314.
5. L.Pan, J. Zou, X. Zhang and L. Wang, *J. Am. Chem. Soc.*, 2011, **133**, 10000-10002.
6. (a) J. G. Yu and J. R. Ran, *Energy Environ. Sci.*, 2011, **4**, 1364 –1371; (b) M. A. Butler and D. S. Ginley, *J. Electrochem. Soc.*,1978, **125**, 228-232.
7. C. Wang, C. Shao, X. Zhang and Y. Liu, *Inorg. Chem.*, 2009, **48**, 7261–7268.

8. (a) Y. Cao, T. He, Y. Chen and Y. Cao, *J. Phys. Chem. C*, 2010, **114**, 3627-3633; (b) J. Zhang, Q. Xu, Z. Feng, M. Li and C. Li, *Angew. Chem. Int. Ed.*, 2008, 47, 1766-1769; (c) V. Etacheri, M. K. Seery, S. J. Hinder and S. C. Pillai, *Chem. Mater*., 2010, **22**, 3843-3853.

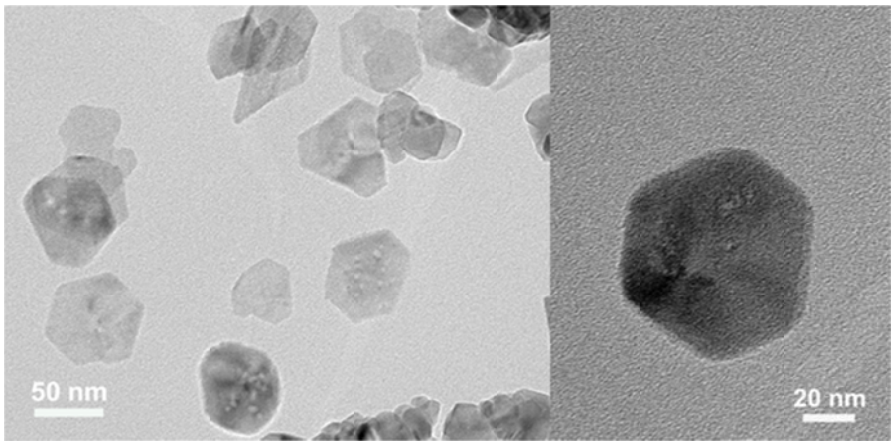

Figure S8. SEM image of the SnS_2 nanosheets.

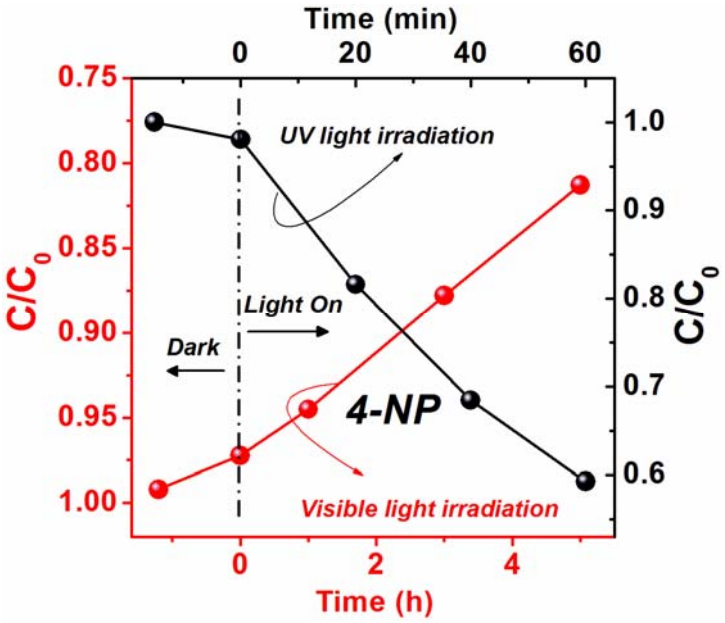

Figure S9. Degradation curves of 4-NP over the physically mixed SnS_2/TiO_2 (AR) under UV and visible light irradiation.

The photocatalytic activities of the physically mixed SnS_2/TiO_2 (AR) were evaluated by the degradation of 4-NP under UV and visible light irradiation, respectively. The physically mixed SnS_2/TiO_2 (AR) was consisted of SnS_2 nanosheets (32.0 wt.%) and TiO_2 (AR) nanofibers (68.0 wt.%), which was similar with the composition of SnS_2/TiO_2 (AR) hierarchical nanostructures. As observed in Figure S9, the physically mixed SnS_2/TiO_2 sample exhibited negligible activity. The photodegradation efficiency of 4-NP just reached about 40.6% after UV light irradiation for 60 min and 18.7% after visible light irradiation for 5h. The results further confirmed that the SnS_2/TiO_2 (AR) hierarchical nanostructures possessed the highest photocatalytic activity in our present work due to the photoinduced interfacial charge transfer based on the photosynergistic effect of SnS_2/TiO_2 heterojunction.